

AniPixel: Towards Animatable Pixel-Aligned Human Avatar

Jinlong Fan
jfan0939@uni.sydney.edu.au
The University of Sydney
Sydney, NSW, Australia

Zhi Hou
zhou9878@uni.sydney.edu.au
The University of Sydney
Sydney, NSW, Australia

Jing Zhang
jing.zhang1@sydney.edu.au
The University of Sydney
Sydney, NSW, Australia

Dacheng Tao
dacheng.tao@gmail.com
The University of Sydney
Sydney, NSW, Australia

ABSTRACT

Although human reconstruction typically results in human-specific avatars, recent 3D scene reconstruction techniques utilizing pixel-aligned features show promise in generalizing to new scenes. Applying these techniques to human avatar reconstruction can result in a volumetric avatar with generalizability but limited animatability due to rendering only being possible for static representations. In this paper, we propose AniPixel, a novel animatable and generalizable human avatar reconstruction method that leverages pixel-aligned features for body geometry prediction and RGB color blending. Technically, to align the canonical space with the target space and the observation space, we propose a bidirectional neural skinning field based on skeleton-driven deformation to establish the target-to-canonical and canonical-to-observation correspondences. Then, we disentangle the canonical body geometry into a normalized neutral-sized body and a subject-specific residual for better generalizability. As the geometry and appearance are closely related, we introduce pixel-aligned features to facilitate the body geometry prediction and detailed surface normals to reinforce the RGB color blending. We also devise a pose-dependent and view direction-related shading module to represent the local illumination variance. Experiments show that AniPixel renders comparable novel views while delivering better novel pose animation results than state-of-the-art methods. Code will be released at AniPixel.

CCS CONCEPTS

• **Human-centered computing** → **Mixed / augmented reality**.

KEYWORDS

Avatar, Human animation, Neural field, Pixel-aligned features

ACM Reference Format:

Jinlong Fan, Jing Zhang, Zhi Hou, and Dacheng Tao. 2023. AniPixel: Towards Animatable Pixel-Aligned Human Avatar. In *Proceedings of the 31st ACM International Conference on Multimedia (MM '23)*, October 29–November 3, MM '23, October 29–November 3, 2023, Ottawa, ON, Canada

Permission to make digital or hard copies of all or part of this work for personal or classroom use is granted without fee provided that copies are not made or distributed for profit or commercial advantage and that copies bear this notice and the full citation on the first page. Copyrights for components of this work owned by others than the author(s) must be honored. Abstracting with credit is permitted. To copy otherwise, or republish, to post on servers or to redistribute to lists, requires prior specific permission and/or a fee. Request permissions from permissions@acm.org.

MM '23, October 29–November 3, 2023, Ottawa, ON, Canada

© 2023 Copyright held by the owner/author(s). Publication rights licensed to ACM.

ACM ISBN 978-x-xxxx-xxxx-x/YY/MM...\$15.00

<https://doi.org/10.1145/nnnnnnnn.nnnnnnnn>

generalizable	animatable	surface normals	learnable lbs	latent codes	deformation	
×	✓	×	×	per-frame	F	NeuralBody [30]
×	✓	×	✓	per-frame	B	AniNeRF [29]
✓	✓	×	×	×	F+B	MPS-NeRF [6]
✓	×	×	×	×	-	KeypointNeRF [22]
✓	✓	✓	✓	per-idx.	F+B	Ours

Table 1: Design differences. F and B mean the **Forward** and **Backward skinning**, respectively. **Per-frame** indicates that the latent code is for each frame while **per-idx** means a latent code for each person. **learnable lbs** indicates if the blend weights are learnable.

2023, Ottawa, ON, Canada. ACM, New York, NY, USA, 10 pages. <https://doi.org/10.1145/nnnnnnnn.nnnnnnnn>

1 INTRODUCTION

Human animation and free-view rendering have a variety of applications such as telepresence, movies, video games, and sports broadcasting [49]. Conventionally, 3D human avatar reconstruction requires expensive setups such as dense multi-view camera rigs or accurate depth sensors [4, 5, 7]. With the recent success of neural radiance field (NeRF) representation [23], a line of works has tried to reconstruct volumetric avatars in radiance field [29, 30, 44]. These neural avatars are human-specific and the model has to be trained from scratch for an unseen person, which is tedious and frustrating in applications. Another line of works leverages pixel-aligned features to reconstruct a generalizable avatar from sparse multi-view images [14, 32–35, 46], which can be tested directly on unseen persons. Although pixel-aligned volumetric avatars can achieve photo-realistic novel-view synthesis for unseen persons, they are limited to *still* humans since the position of query points under the target pose must be the same as that of the ones used to extract the pixel-aligned features under the input pose, which prevents volumetric avatar from pose-controllable animation.

In this work, our goal is to make the pixel-aligned human avatar animatable, whilst preserving its capability to generalize to previously unseen persons, as well as facilitating decent-quality rendering when generating novel views using sparse multi-view images. However, there is a significant challenge, i.e., how to align the dynamic points in the target space to the input space. Some recent works extend NeRF with a non-rigid deformation field to represent dynamic scenes [27, 31, 40] but jointly learning NeRF and the deformation field is ill-posed and prone to local minima [16, 29]. For

human reconstruction, skeleton motion is often taken as prior to constraining the deformation field [29, 30, 50]. As these methods commonly render the body directly from the canonical space, they only focus on the deformation from observation space to canonical space. But in our setting, the pixel-aligned features are extracted in a separate input space, which makes the problem more challenging. To deal with that, we devise a bidirectional neural skinning field that enables both target-to-canonical and canonical-to-observation deformation. Meanwhile, we also leverage human priors in the learning process to optimize the deformation field [15, 19].

Nevertheless, the diverse body shapes and appearances among different persons pose significant challenges to appealing animatable pixel-aligned avatars. To attain better generalization capability and reconstruct more geometry details, we devise a canonical body and disentangle it into the human-shared neutral part and a subject-specific part. Humans share similar body structures, but each person also has a unique body shape, appearance, style of dress, etc. The shared part in our method is represented as a normalized neutral-sized body and the subject-specific part is described by a residual displacement field. On the other hand, for appearance reconstruction, blending weights are predicted using the fused pixel-aligned features [42]. In existing methods, the blended colors are pose-independent, but in our setting, the target pose can be different from the input pose. To that end, we incorporate a shading module to predict a per-point scalar shading factor to modulate the blended colors for representing the pose-related local illumination. Combining the appearance module with the canonical geometry module, we can generate a holistic volumetric avatar.

We evaluate our Animatable Pixel-aligned human avatar dubbed AniPixel, on the Human3.6M [10] and ZJUMoCap [30] datasets that provide synchronized multi-view video sequences of dynamic humans. Both for the novel view synthesis and novel pose animation, AniPixel exhibits state-of-the-art performance, and surprisingly outperforms human-specific methods on the animation task.

In summary, our method reconstructs a volumetric human avatar that is both animatable and generalizable. Novel views of unseen persons in novel poses can be directly rendered from sparse multi-view images, which is of great practical significance in real-world applications. The contribution of this paper is three-fold. 1) We devise a bidirectional neural skinning field and a neutralized canonical space to align the target pose with the input pose, making the pixel-aligned human avatar animatable. 2) We represent generalizable human body geometry by disentangling it into a neutral-sized shared body and a subject-specific residual field for better generalizability. 3) We leverage an extra shading module to modulate the RGB color to better represent the local illumination variance. Our method can render even better results in novel view and novel pose for unseen persons than human-specific methods.

2 RELATED WORK

Neural rendering. Recently, various neural scene representations have been presented for novel view synthesis [18, 37] and geometric reconstructions [21, 26]. In particular, NeRF [23] that combines MLPs with differentiable volumetric rendering achieves photo-realistic view synthesis. Standard NeRF needs per-scene optimization making it expensive for real-life applications. A bunch of following works have tried to advance it with generalizability [2, 41, 42, 48]

so that the trained model can directly synthesize novel views of novel scenes from the multi-view input images without re-training. In these works, the pixel-aligned features-based technique often plays a fundamental role. However, it can only work on static scenes, e.g., for rendering humans [25, 34, 35, 50], the person is required to be still. In this paper, we devise a bidirectional neural skinning field and a neutral canonical space to make the pixel-aligned features adaptive to dynamic humans and the reconstructed volumetric avatar animatable.

Human animation. As a common approach, skeletal animation [12, 15] combines skeleton and per-vertex blend weight to animate a human mesh. Based on the Skinned Multi-Person Linear model (SMPL) [19], the human mesh can be animated with SMPL parameters fitted from images [17, 38]. However, SMPL can only describe naked persons and can not directly render photo-realistic images. Recent works integrate SMPL with NeRF to capture human clothing and hair [8, 9, 45]. To account for dynamic humans, deformation fields are devised to deform the posed body in target space to canonical space, where the density and color are predicted [29, 30]. To ensure stability during training, human priors are often introduced [44] or used to initialize the motion field [6, 30, 51]. In Dual-NeRF [51], the radiance field of the canonical body and the lighting conditions in the world space is represented separately using MLPs, resulting in a more accurate depiction of pose-dependent color effects. The reconstructed volumetric avatar in the canonical space can be driven by novel poses and render novel view images. However, these models are human-specific and have to be trained from scratch for each new subject. In recent research, attempts have been made to reconstruct generalizable avatars [3, 14]. NHP [14] employs a Temporal Transformer for aggregating skeletal features and a Multi-view Transformer for fusing time-augmented features. GNR [3] proposes an extra occlusion-aware appearance blending module to guide the blending of appearances from source views. Similarly, our approach shares the same objective. By utilizing a multi-person shared canonical body and pixel-aligned appearance features, our method demonstrates the ability to generalize to unseen individuals. The most related work to our method is MPS-NeRF [6], which directly utilizes skeleton-driven deformation to align humans and the canonical geometry is an SMPL body. In contrast, we use learnable skinning fields to align the points and supplement a neutral-sized shared body with a residual field to depict the dynamic body. Besides, the RGB colors in MPS-NeRF are predicted using fused features, while our method outputs the colors by blending input ones, which has been proven more efficient [42]. We also take into account the local illumination variance in color rendering.

3 METHOD

We propose AniPixel which can directly render realistic images of an unseen person in novel views and novel poses taking only multi-view images as input. For the input multi-view images, we assume the calibration parameters and the foreground human mask are known. We also assume the parameters of a 3D human parametric model are fitted both for the target pose and the input pose. We use SMPL as our parametric model. The 3D joints for the input pose are also regressed.

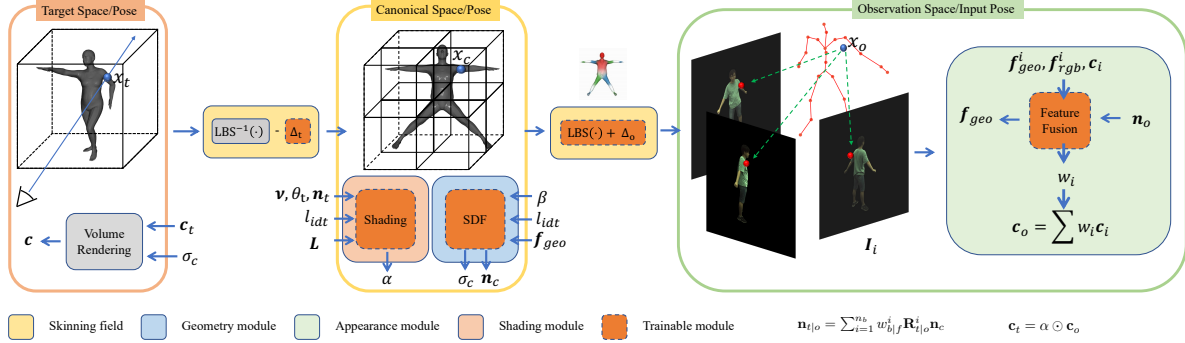


Figure 1: Method overview. We propose AniPixel, an animatable and generalizable method that only takes sparse multi-view images as input. Specifically, our method includes four modules: a) Skinning field module outputs a bidirectional neural skinning field to align the target pose and the input pose with the canonical pose, which integrates skeleton-driven deformation with a learnable blending weight field. Given query points x_t in target space, they are first transformed to the canonical space as x_c via the backward skinning and then to the observation space as x_o via the forward skinning; b) Canonical Geometry Module represents body geometry in the canonical pose as an SDF which is shared by multiple persons. For better generalizability, we disentangle the canonical body geometry to a neutral-sized body and a pose-dependent and human-specific residual displacement field Δ ; c) Appearance Module blends RGB colors c_i from the input images I_i to colors c_o for points x_o in the observation space; d) Shading Module leverages scalar shading factor α to modulate the output color c_o to represent the local illumination variance. Final RGB colors c according to the target points x_t is accumulated through volume rendering.

The overview of the proposed method is illustrated in Figure 1. Following the rendering scheme of NeRF [20, 23], we cast rays to the target space which pass the camera center and the pixel, and then sample points along the rays. The sampled points x_t in target pose are first transformed to the canonical space as x_c , and then to the observation space as x_o via the bidirectional skinning field which is based on skeleton-driven deformation and neural blend weight field (Section 3.1). The body geometry is stored in a canonical neural field (Section 3.2) and appearance information of x_t is derived from input images using pixel-aligned features (Section 3.3). An extra shading module is leveraged to represent the local illumination variance (Section 3.4). The final color c is accumulated through differentiable volume rendering [11].

3.1 Bidirectional Skinning Field

To align the target pose with the input pose, we propose a bidirectional skinning field including a backward skinning field to transform points in the target space to the canonical space and a forward skinning field to transform the canonical points to the observation space. We use the linear blend skinning (LBS) [15] as the skinning algorithm. But the original LBS weights are only defined on SMPL mesh points. Generally, there are two ways to diffuse the weights to any 3D point. One way is to assign the weight using its nearest neighbor (NN) on the SMPL mesh or through barycentric interpolation of Top-k closest vertices [6, 30, 43]. The other way is to predict the per-point weights using a neural network [17, 29, 44]. Learnable blend weights are more flexible and can represent non-rigid deformation more precisely. However, we found that if the backward and forward blend weights are both learnable and optimized simultaneously, the training would be unstable and hard to

converge. So in this work, we devise the backward weights field as a deterministic NN field and the forward one as a learnable neural field, which demonstrate adequate capacity in our experiment.

Backward skinning. Given sampling points x_t in the target space and the target pose parameters θ_t , we first calculate the bone transformations $B_t = \{B_t^i\}_{i=1}^{24}$ corresponding to pose θ_t . Each B^i is a 4×4 rotation-translation matrix. The skinning weight vector is defined as $w_b \in [0, 1]^{25}$, s.t. $\sum_{i=1}^{25} w_b^i = 1$. Note that here we add an extra blend weight w_{bg} for static background points [44], so the skinning field can represent both the foreground and background motions. The background weights are calculated as $w_{bg} = 1 - \sum_{i=1}^{24} w_{fg}^i$. For each point in space, we assign the skinning weights of its NNs on the body surface, and if the closest distance is greater than a threshold we assume it is a background point and set $w_{fg}^i = 0$, $w_{bg} = 1$. For subject-specific geometry that can not be shared in the canonical body, e.g., clothes and hair, we model the residual as a displacement field and implement it as an MLP network $F_{\sigma_d} : (\phi(x), l_{idt}, \theta) \mapsto \Delta$, where σ_d is the network parameters and Δ is the per-point displacement, l_{idt} is the per-identity latent code and $\phi(\cdot)$ is the position encoding function [39]. Combining the skinning field with the displacement field, we can transform points x_t as:

$$\begin{aligned} x_c &= LBS(x_t)^{-1} - \Delta_t \\ &= \left(\sum_{i=1}^{n_b} w_b^i(x_t, S_t) \cdot B_t^i(\theta_t, \theta_c) \right)^{-1} \cdot x_t - \Delta_t, \end{aligned} \quad (1)$$

where S_t is the target SMPL parameters, $n_b = 25$, θ_c denotes the canonical pose parameters, and Δ_t is the displacement regarding to target pose θ_t .

Implicit forward skinning. The pixel-aligned features are sampled by projecting 3D points to the 2D feature maps, so the results are sensitive to the position of 3D points. In order to align the canonical points with the corresponding ones in the observation space more precisely, we use a neural blend weight field in forward skinning. As this weight field is multi-person shared, we also condition it on l_{idt} . We implement it as a separate MLP network $F_{\sigma_w} : (\phi(\mathbf{x}_c), l_{idt}) \mapsto \mathbf{w}_f$. However, the weight field (\mathbf{w}_f) is under-constrained, and jointly learning with the neural field is prone to local minima [16, 29]. To deal with that, we initialize the blend weight field with the pre-defined values \mathbf{w}_{init} in the SMPL model. The forward skinning weights are generated via the softmax activation function:

$$\mathbf{w}_f(\mathbf{x}_c) = \text{softmax}(F_{\sigma_w}(\phi(\mathbf{x}_c), l_{idt}) + \log(\mathbf{w}_{init}(\mathbf{x}_c))). \quad (2)$$

When transforming points from the canonical space into the observation space, we need to add back the human-specific displacement:

$$\begin{aligned} \mathbf{x}_o &= LBS(\mathbf{x}_c) + \Delta_o \\ &= \sum_{i=1}^{n_b} \mathbf{w}_f^i(\mathbf{x}_c) \cdot \mathbf{B}_o^i(\theta_c, \theta_o) \cdot \mathbf{x}_c + \Delta_o, \end{aligned} \quad (3)$$

where Δ_o is the displacement regarding to input pose θ_o .

3.2 Canonical Geometry Module

For a specific person, we can disentangle its body geometry into a multi-person shared part and a residual part. The latter is modeled as the displacement field Δ and the former is stored in a canonical neural field. When shared by multiple persons, the canonical field should have the ability to distinguish the geometry difference between each subject, e.g., bone length. Utilizing the shape parameters β from the SMPL model, we can represent the body shape approximately, e.g., fat or slim. More than that, we condition the neural field on per-identity latent code l_{idt} for the other variations, e.g., the shape of shoes. To make learning easier, we also resize the body of each person to align with a pre-defined neutral-sized canonical body via the minimum 3D bounding box of the SMPL mesh. The pixel-aligned features from the observation space can provide significant clues for geometry prediction, so we also condition the neural field on the fused pixel-aligned features. The canonical neural field is defined as a signed distance field (SDF) [47] and HashGrid [24] is taken as the position encoding method. An MLP is used to predict the SDF: $F_{\sigma_s} : (\phi(\mathbf{x}_c), \beta, l_{idt}, \mathbf{f}_{geo}) \mapsto s$, where \mathbf{f}_{geo} is the geometry features. Given a point \mathbf{x}_c in the canonical space, its SDF is:

$$s = F_{\sigma_s}(\phi(\mathbf{x}_c), \beta, l_{idt}, \mathbf{f}_{geo}), \quad (4)$$

where $\phi(\cdot)$ is the HashGrid position encoding function.

Given the SDF, surface normals \mathbf{n}_c can be calculated as $\mathbf{n}_c = \nabla F_{\sigma_s} / \|\nabla F_{\sigma_s}\|_2$, where gradient ∇F can be obtained by network backpropagation. And the surface normal vectors are transformed to the target and observation space by using the rotational part of the backward skinning and forward skinning respectively: $\mathbf{n}_{t|o} = \sum_{i=1}^{n_b} \mathbf{w}_{b|f}^i \mathbf{R}_{t|o}^i \mathbf{n}_c$. Following the SDF-based volume rendering formulation [47], we convert SDF values into density values σ using the scaled CDF of the Laplace distribution:

$$\sigma = \frac{1}{b} \left(\frac{1}{2} + \frac{1}{2} \text{sign}(s) \exp\left(-\frac{|s|}{b}\right) - 1 \right), \quad (5)$$

where b is a learnable parameter.

3.3 Appearance Module

Following [42], we utilize pixel-aligned features from the sparse multi-view input images in the observation space to blend RGB colors, making the appearance module generalizable and requiring only sparse input views.

Given the transformed 3D query points \mathbf{x}_o , we project them onto the input images I_i and the extracted feature maps F_i by perspective projection $\Pi(\mathbf{x}_o | \mathbf{P}_i)$. The pixel-aligned colors \mathbf{c}_i and features \mathbf{f}_i are sampled through bilinear interpolation. Considering the camera rays in the target space are bent after being transformed to the observation space, unlike [22], we do not directly take the target view directions as input to represent the view-dependent effects. Instead, we introduce the detailed surface normals to better indicate the per-point directions and describe the view-related effects as a shading factor (Sec. 3.4). Similar to [42], we output the RGB color \mathbf{c}_o as a weighted sum of all the input colors \mathbf{c}_i , and the blending weights for each input view are predicted using a feature fusion function $F_{\sigma_c} : (\phi'(\mathbf{x}_o, \mathbf{J}_o), \mathbf{f}_{geo}^i, \mathbf{f}_{rgb}^i, \mathbf{c}_i, \mathbf{n}_o) \mapsto (w_i, \mathbf{f}_{geo})$, where \mathbf{f}_{geo}^i and \mathbf{f}_{rgb}^i are the input geometry and appearance features for i th view, $\phi'(\cdot)$ is relative spatial encoding function [22], w_i is the output blending weights for i th view, s.t. $w_i \in [0, 1]$ and $\sum w_i = 1$. We also output the fused geometry features \mathbf{f}_{geo} to facilitate the canonical geometry reconstruction. Please see the supplemental material for further architectural details. The blended color \mathbf{c}_o can be written as:

$$\mathbf{c}_o = \sum w_i \mathbf{c}_i = \sum F_{\sigma_c}(\mathbf{f}_{geo}^i, \mathbf{f}_{rgb}^i, \mathbf{c}_i, \mathbf{n}_o) \mathbf{c}_i. \quad (6)$$

3.4 Shading Module

As the appearance information derived from the observation space is in the input pose, which is different from the target pose. When the human pose changes, local illumination on the body surface may also change, e.g., if lifting arms to the head, there might be shading on the face. Besides, the colors in the observation space are not conditioned on the target view directions \mathbf{v} , so the output colors \mathbf{c}_o are not view-dependent, which is undesirable for realistic rendering. To tackle this problem, we devise a shading module predicting a pose-dependent and view direction-related per-point scalar shading factor to modulate the output colors \mathbf{c}_o . To capture subject-specific effects, e.g., different reflectance caused by variant clothes materials, we also take the identity latent code l_{idt} as conditional input. Additionally, during the data collection process, the captured images are obtained over a period of time, during which environmental illumination and camera settings may change. Inspired by [1], we extract a global feature \mathbf{L} from the input images to account for the overall per-image illumination variance. In a nuts shell, the shading module aims to accurately represent the per-image, subject-specific, pose-dependent, and view-dependent color factors. We use a shallow MLP to predict the shading factor $F_{\sigma_l} : (\mathbf{v}, \theta_t, \mathbf{n}_t, l_{idt}, \mathbf{L}) \mapsto \alpha$. The modulated color is:

$$\mathbf{c}_t = \alpha \odot \mathbf{c}_o = F_{\sigma_l}(\mathbf{v}, \theta_t, \mathbf{n}_t, l_{idt}, \mathbf{L}) \odot \mathbf{c}_o, \quad (7)$$

where \odot means per-point multiplication. Through this shading factor modulation, the appearance information in observation space

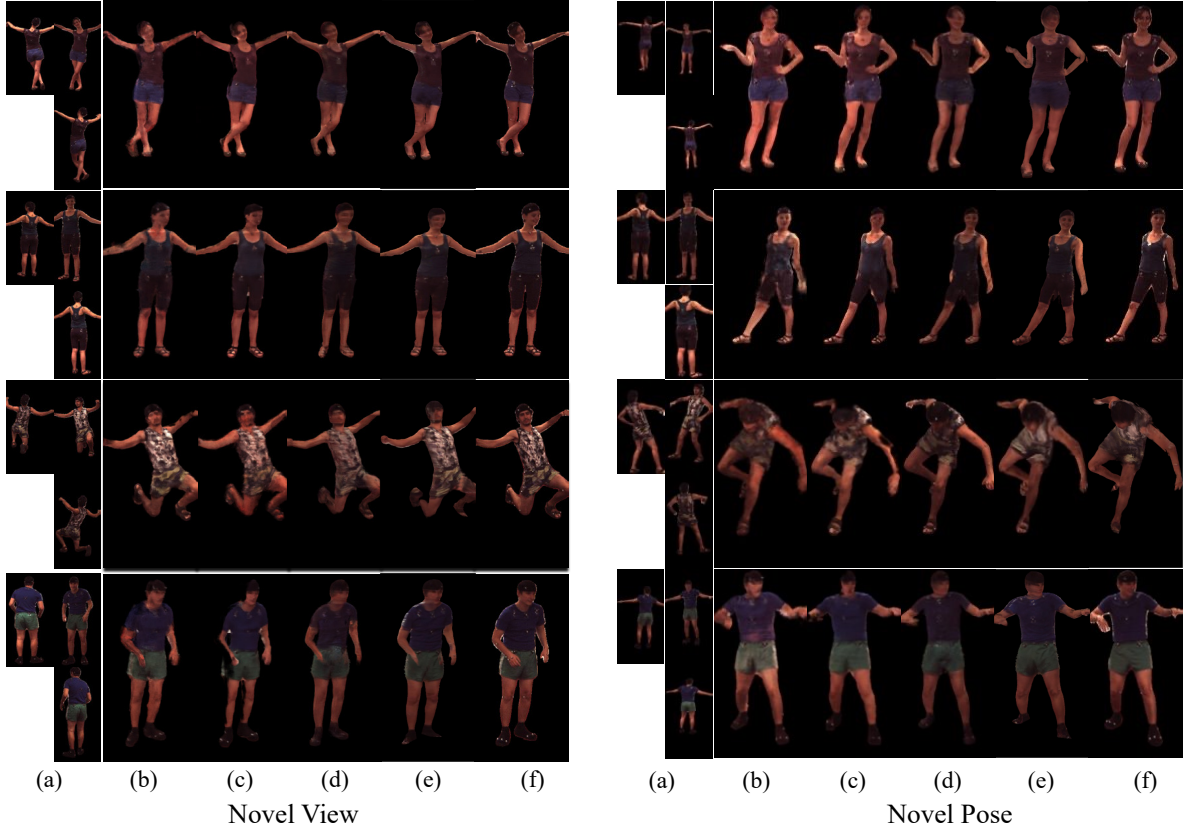


Figure 2: Novel view and novel pose rendering results on the Human3.6M dataset. For each part, there are (a) the input three views and results of (b) AniNeRF [29], (c) NeuralBody [30], (d) MPS-NeRF [6], (e) our method, and (f) the ground truth. NeuralBody and AniNeRF are human-specific methods and do not need multiple input views in testing. The results in the above two settings are rendered given the target camera parameters and novel pose parameters, respectively.

Subject	Novel View Synthesis								Novel Pose Synthesis							
	PSNR				SSIM				PSNR				SSIM			
	NB	AniNeRF	MPS	Ours	NB	AniNeRF	MPS	Ours	NB	AniNeRF	MPS	Ours	NB	AniNeRF	MPS	Ours
S1	22.87	22.05	25.40	<u>25.15</u>	0.897	0.888	0.926	<u>0.912</u>	<u>22.11</u>	21.37	21.87	24.60	0.879	0.868	<u>0.880</u>	0.896
S5	<u>24.60</u>	23.27	24.30	24.63	0.917	0.892	<u>0.908</u>	0.894	<u>23.51</u>	22.29	21.49	24.19	0.897	0.875	0.871	<u>0.883</u>
S6	22.82	21.13	<u>23.94</u>	24.49	0.888	0.854	<u>0.893</u>	0.897	<u>23.52</u>	22.59	<u>23.63</u>	23.85	0.889	0.884	<u>0.891</u>	0.894
S7	23.17	22.50	<u>24.27</u>	24.60	0.914	0.890	<u>0.911</u>	0.901	<u>22.33</u>	22.22	21.88	23.87	0.889	0.878	0.868	<u>0.884</u>
S8	21.72	22.75	<u>23.66</u>	24.41	0.894	<u>0.898</u>	0.920	0.895	20.94	<u>21.78</u>	21.15	24.03	0.876	0.882	<u>0.888</u>	0.892
S9	24.28	<u>24.72</u>	24.55	25.87	<u>0.910</u>	0.908	0.899	0.918	23.04	<u>23.72</u>	23.33	24.83	0.884	<u>0.886</u>	0.875	0.904
S11	23.70	24.55	25.12	<u>24.95</u>	0.896	0.902	0.913	<u>0.905</u>	23.72	<u>23.91</u>	23.53	24.06	0.884	0.889	<u>0.891</u>	0.895
Average	23.31	23.00	<u>24.06</u>	24.87	<u>0.903</u>	0.890	0.910	<u>0.903</u>	<u>22.74</u>	22.55	22.41	24.20	<u>0.885</u>	0.880	0.881	0.893

Table 2: Comparison of our method with NeuralBody [30], AniNeRF [29], MPS-NeRF [6] on the Human3.6M dataset. The best and second-best results are marked in bold and underlined, respectively.

is adapted to the target space. Given the density and RGB color for each query point on a ray $\mathbf{r} = (\mathbf{c}_t, \sigma)$, we render the pixel color using standard volume rendering [23].

3.5 Training Loss

Our method is end-to-end trainable and all the modules are optimized jointly. The training loss is defined as:

$$\mathcal{L} = \lambda_C \mathcal{L}_C + \lambda_M \mathcal{L}_M + \lambda_N \mathcal{L}_N + \lambda_S \mathcal{L}_S + \lambda_D \mathcal{L}_D. \quad (8)$$

where \mathcal{L}_C is the color loss. Specifically, given the ground truth target image and predicted one, we apply l_1 -distance loss and VGG

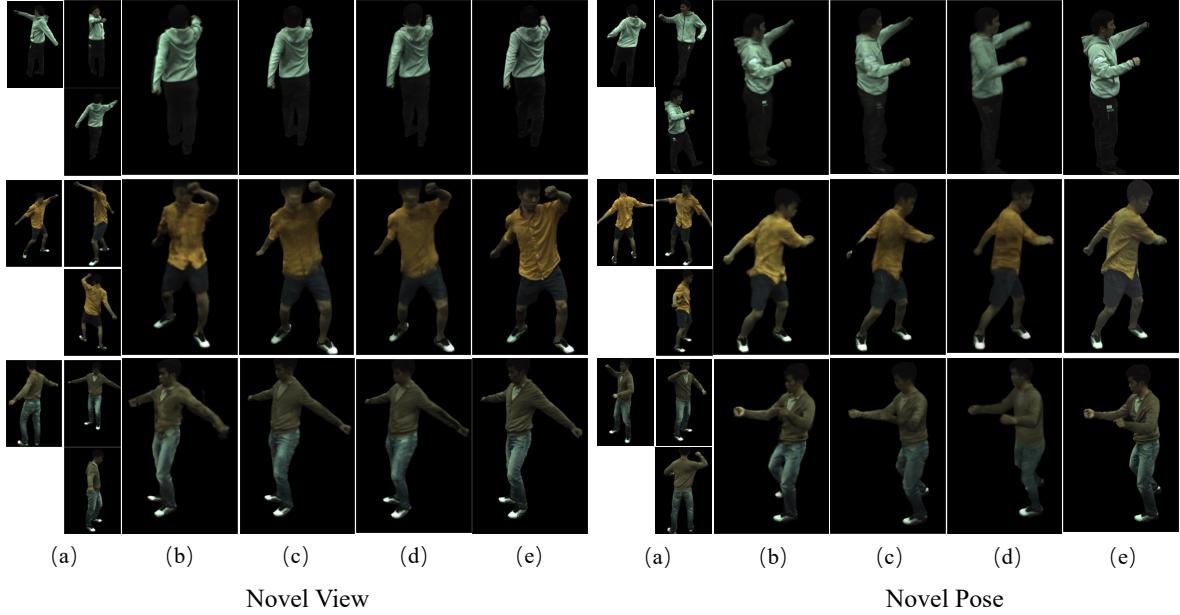


Figure 3: Novel view and novel pose synthesis results on the ZJUMoCAP dataset. For each part, there are (a) the input three views and results of (b) NeuralBody [30], (c) KeypointNeRF [22], (d) our methods, and (e) the ground truth. NeuralBody and AniNeRF are human-specific methods. The results in the above two settings are rendered given the target camera parameters and novel pose parameters, respectively. Since KeypointNeRF is not animatable, we set the input pose to be the same as the target one during testing.

Method	Novel View		Novel Pose	
	PSNR	SSIM	PSNR	SSIM
Human-specific:				
NeuralBody	28.90	0.967	23.06	0.879
AniNeRF	27.10	0.949	23.16	0.893
Generalizable:				
KeypointNeRF	25.03	0.896	N/A	N/A
Ours	26.39	0.911	24.87	0.895

Table 3: Comparison of NeuralBody [30], AniNeRF [29], KeypointNeRF [22], and our method on ZJUMoCAP. NeuralBody and AniNeRF are human-specific methods while KeypointNeRF and our method are generalizable. KeypointNeRF requires the target pose and input pose to be the same and is not applicable to the novel pose setting.

perception loss [36] to supervise the training. \mathcal{L}_M is the mask loss. We predict two versions of masks, one is rendered by volume density accumulation, and the other is generated by minimum SDF rendering as in [29]. \mathcal{L}_N is surface normal regularization, including smoothness loss and shape loss defined the same as in [6]. \mathcal{L}_S is the Eikonal loss to make sure the neural field is prone to be an SDF. The gradients of the neural fields are calculated conveniently using the automatic differentiation tool in PyTorch [28]. \mathcal{L}_D is l_2 -norm regularization of the displacement fields, including both the forward and backward skinning fields, encouraging the residual displacement to be as small as possible. λ_C , λ_M , λ_N , λ_S and λ_D are loss weights to balance these loss terms. Please refer to the supplement for their settings.

4 EXPERIMENTAL RESULTS

Implemental details. We use the Adam optimizer [13] with a learning rate of $5e^{-4}$ and a batch size of 1 to train the network. To initialize the SDF, we first train 30K iterations with only the \mathcal{L}_M loss and then train another 120K iterations with all the losses. In order to use VGG loss to capture high-frequency details, we render patches instead of random rays [22]. The center of the patch is randomly sampled in the minimum bounding rectangle area of the foreground mask and the query points are sampled from the 3D bounding box derived from the SMPL model. Along each ray, 64 points are sampled for coarse rendering and 16 points for fine rendering. l_{idt} is selected as the nearest person for testing. We use four Nvidia Tesla V100 GPUs for training and it takes about one day to converge. More details are provided in the supplementary material.

Datasets. We mainly evaluate our method and compare it with other methods on two public datasets. The first one is the Human3.6M dataset [10], which contains 4-view sequences of different actors. Following [6, 29], we conduct experiments on 7 subjects: S1, S5, S6, S7, S8, S9 and S11. We test our method using the same setting as [6] for a fair comparison. The second dataset is the ZJU-Mocap dataset [30], which provides video sequences of 10 subjects captured from 23 synchronized cameras. The splitting of training and test set is the same as [22].

Evaluation metrics. We use PSNR and SSIM metrics for quantitative evaluation. Instead of directly calculating PSNR and SSIM

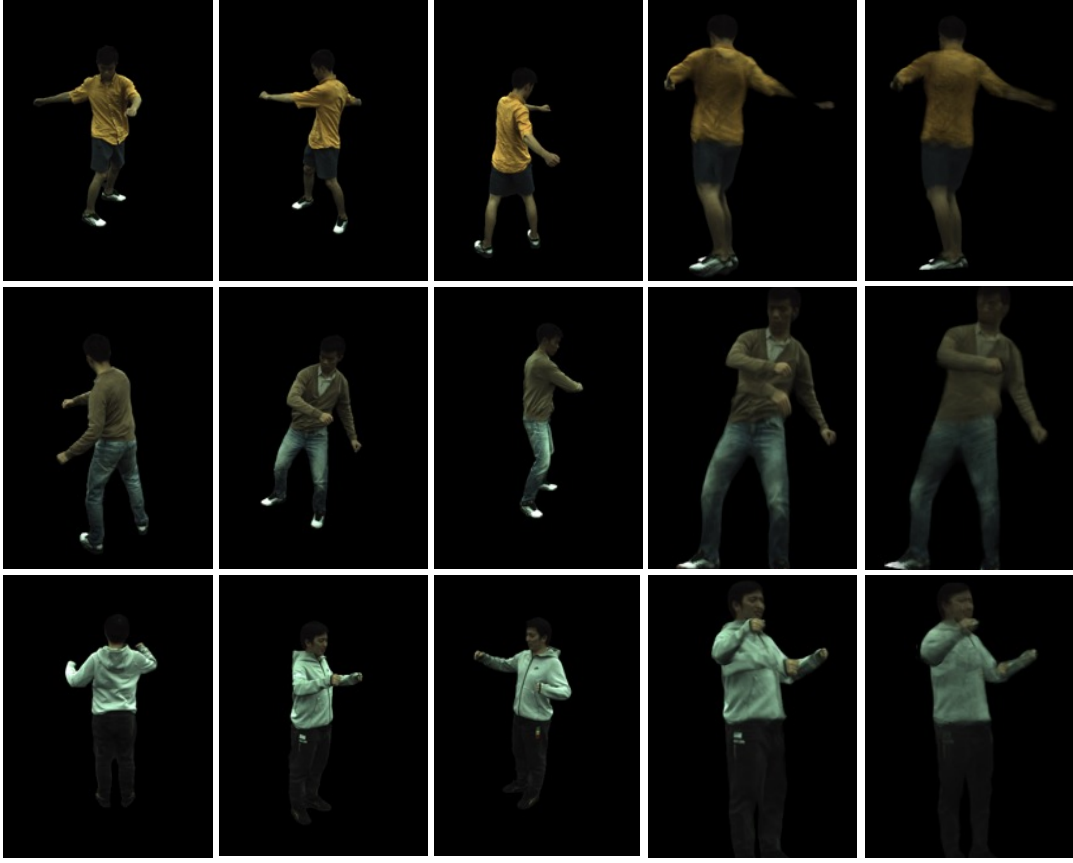


Figure 4: Comparison with KeypointNeRF [22] on novel view synthesis. First three columns are input views. The fourth column is the result of KeypointNeRF and the fifth column is the result of our AniPixel. Input poses are the same as target ones following KeypointNeRF’s setting.

for the whole image, we follow previous methods [6, 29, 30] to project the 3D bounding box of the fitted SMPL mesh onto the image plane to obtain a 2D mask and only calculate PSNR and SSIM in the masked region.

4.1 Comparison with previous methods

Baselines. We compare our method with recent two animatable methods, NeuralBody [30] and AniNeRF [29], and two generalizable methods, KeypointNeRF [22] and MPS-NeRF [6]. NeuralBody and AniNeRF are human-specific models that require training a single model for each subject. In evaluation, camera parameters and pose parameters are used to animate the learned neural field. KeypointNeRF and MPS-NeRF can generalize to unseen persons taking multi-view images as input. But KeypointNeRF only works in static scenes and is not applicable to animation tasks.

Results on Human3.6M. Table 2 presents the quantitative comparison of our AniPixel with the other three methods. For novel view synthesis, our method has marginally higher PSNR on average and

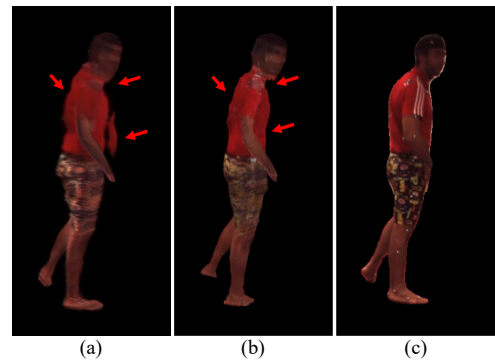


Figure 5: Visual results of (a) MPS-NeRF and (b) our AniPixel as well as (c) the ground truth.

comparable SSIM with other methods, which confirms the valid reconstruction of the canonical body geometry in our method. In the animation task, both our AniPixel and MPS-NeRF are tested on unseen persons. NeuralBody and AniNeRF are trained and tested on the same person. Our method outperforms all three methods both in PSNR and SSIM. Note that since AniPixel is both animatable and generalizable, it obtains about 2dB higher PSNR on average than MPS-NeRF, which we attribute to the effectiveness of the proposed neural skinning field and residual displacement field.

Visual results are shown in Figure 2. It can be observed that our method can render competitive results both on novel views and unseen persons in novel poses. Our results of S6 in novel view synthesis (*i.e.*, third row in left part) and S1 in novel pose synthesis (*i.e.*, first row in right part) show better pixel lightness than MPS-NeRF, owing to the proposed shading module for modeling local illumination variance. Based on the bidirectional skinning field, our method can also align the poses more precisely as demonstrated in Figure 5. Video demo and more visual results are included in the supplementary material.

Results on ZJUMoCap. The quantitative results and rendering results compared with NeuralBody and KeypointNeRF are listed in Table 3 and shown in Figure 3 respectively. Not that NeuralBody is a human-specific method and takes target camera parameters to render novel view images and pose parameters to synthesize novel pose images. KeypointNeRF is only applicable to static humans and the input pose should be selected to be the same as the target one, while our method takes a different pose from the target pose as input. Even under a more challenging setting, our AniPixel can still output comparable visual results on novel view synthesis and novel pose synthesis with other methods and even obtains higher objective results (*e.g.*, about 1.8dB higher PSNR) on novel pose synthesis than the human-specific methods.

Self-occlusion artifacts. In KeypointNeRF [22], for each pixel in the target image, the pixel color is calculated as the blending of input ones, and the blending weights are predicted based on pixel-aligned features. However, all sampled query points on one target ray share the same pixel-aligned features. The relative spatial encoding of each point may result in varying weights between them. But the slightly different weights in empty space still have a chance to output floating artifacts in self-occlusion areas. Some examples are shown in Figure ???. In contrast, thanks to the explicit geometry reconstruction in canonical space, our model has the ability to distinguish empty space from the human body, which can remove floating artifacts effectively, as shown in the last column in Figure ??.

4.2 Ablation studies

We conduct ablation studies on the S9 subject from the Human3.6M dataset. Results are listed in Table 4. When conducting ablation studies on the shading module and residual displacement fields, we simply remove them from the model. For geometry features and human identity latent code, we replace them with constant values. To verify the effectiveness of utilizing surface normals to reinforce the RGB color blending, we replace the normals with target view

	Novel View		Novel Pose	
	PSNR	SSIM	PSNR	SSIM
w/o geo. feats	24.07	0.870	22.33	0.832
w/o normals	23.98	0.881	22.72	0.845
w/o shading	23.88	0.889	22.82	0.884
w/o displacement	24.56	0.879	23.21	0.848
w/o identity	24.54	0.875	23.34	0.863
w/o learnable skinning	24.29	0.886	24.01	0.847
Our AniPixel	25.81	0.902	24.83	0.895

Table 4: Ablation study of the design choices in our model.



Figure 6: Geometry of (a) MPS-NeRF and (b) our AniPixel in the canonical space.

directions. For the learnable skinning field, it is replaced with the standard skeleton motion.

For novel view synthesis, the shading module plays an important role and the test metrics drop a lot without it. The detailed surface normals transformed from canonical space indeed benefit the color blending in observation space and including it in the model delivers higher metrics. For novel pose synthesis, geometry features show the most important impact which indicates that appearance information could be a valuable clue for geometry reconstruction. The identity latent code and displacement field benefit novel pose synthesis more than the novel view synthesis. And the identity latent code can further promote the results for both tasks.

4.3 Canonical geometry

In order to validate the effectiveness of our canonical SDF, we visualize the learned body geometry of both our method and MPS-NeRF in the canonical space, as shown in Figure 6. Compared with MPS-NeRF, the 3D canonical geometry reconstructed by our method is more complete on arms. It is because MPS-NeRF only depends on the SMPL model to constrain the shape reconstruction, which usually can not well fit the hands. In contrast, our AniPixel can reconstruct the holistic body geometry well based on the residual displacement field and the learnable skinning field.

5 CONCLUSION

We proposed an animatable and generalizable volumetric human avatar reconstruction method that could render novel views and novel poses for unseen persons from sparse multi-view images. Specifically, we devise a bidirectional neural skinning field and a neutralized canonical space to bridge the target pose and the input pose. Meanwhile, a shading module is introduced to improve

the local illumination variance representation. Experiments on the Human3.6M and ZJU MoCap datasets demonstrate that the proposed approach achieves state-of-the-art performance on novel view synthesis and novel pose synthesis, and even outperforms human-specific methods on animation tasks.

Acknowledgement: This work was supported by ARC FL-170100117 and IH-180100002.

REFERENCES

- [1] Thiemo Alldieck, Mihai Zanfir, and Cristian Sminchisescu. 2022. Photorealistic Monocular 3D Reconstruction of Humans Wearing Clothing. In *CVPR*. 1506–1515.
- [2] Anpei Chen, Zexiang Xu, Fuqiang Zhao, Xiaoshuai Zhang, Fanbo Xiang, Jingyi Yu, and Hao Su. 2021. Mvsnerf: Fast Generalizable Radiance Field Reconstruction from Multi-View Stereo. In *ICCV*. 14124–14133.
- [3] Wei Cheng, Su Xu, Jintan Piao, Chen Qian, Wayne Wu, Kwan-Yee Lin, and Hongsheng Li. 2022. Generalizable Neural Performer: Learning Robust Radiance Fields for Human Novel View Synthesis. *arXiv preprint arXiv:2204.11798* (2022). arXiv:2204.11798
- [4] Alvaro Collet, Ming Chuang, Pat Sweeney, Don Gillett, Dennis Evseev, David Calabrese, Hugues Hoppe, Adam Kirk, and Steve Sullivan. 2015. High-Quality Streamable Free-Viewpoint Video. *ACM Transactions on Graphics (ToG)* 34, 4 (2015), 1–13.
- [5] Mingsong Dou, Sameh Khamis, Yury Degtyarev, Philip Davidson, Sean Ryan Fanello, Adarsh Kowdle, Sergio Orts Escolano, Christoph Rhemann, David Kim, and Jonathan Taylor. 2016. Fusion4d: Real-time Performance Capture of Challenging Scenes. *ACM Transactions on Graphics (ToG)* 35, 4 (2016), 1–13.
- [6] Xiangjun Gao, Jiaolong Yang, Jongyoo Kim, Sida Peng, Zicheng Liu, and Xin Tong. 2022. MPS-NeRF: Generalizable 3D Human Rendering From Multiview Images. *TPAMI* PP (Sept. 2022).
- [7] Kaiwen Guo, Peter Lincoln, Philip Davidson, Jay Busch, Xueming Yu, Matt Whalen, Geoff Harvey, Sergio Orts-Escolano, Rohit Pandey, and Jason Dourgarian. 2019. The Relightables: Volumetric Performance Capture of Humans with Realistic Relighting. *ACM Transactions on Graphics (ToG)* 38, 6 (2019), 1–19.
- [8] Tong He, Yuanlu Xu, Shunsuke Saito, Stefano Soatto, and Tony Tung. 2021. ARCH++: Animation-ready Clothed Human Reconstruction Revisited. In *ICCV*. 11046–11056.
- [9] Zeng Huang, Yuanlu Xu, Christoph Lassner, Hao Li, and Tony Tung. 2020. Arch: Animatable Reconstruction of Clothed Humans. In *CVPR*. 3093–3102.
- [10] Catalin Ionescu, Dragos Papava, Vlad Olaru, and Cristian Sminchisescu. 2013. Human3.6m: Large Scale Datasets and Predictive Methods for 3d Human Sensing in Natural Environments. *TPAMI* 36, 7 (2013), 1325–1339.
- [11] James T. Kajiya and Brian P. Von Herzen. 1984. Ray Tracing Volume Densities. *ACM SIGGRAPH Computer Graphics* 18, 3 (1984), 165–174.
- [12] Ladislav Kavan, Steven Collins, Jiri Zára, and Carol O’Sullivan. 2007. Skinning with Dual Quaternions. In *Proceedings of the 2007 Symposium on Interactive 3D Graphics and Games*. 39–46.
- [13] Diederik P. Kingma and Jimmy Ba. 2015. Adam: A Method for Stochastic Optimization. In *ICLR (Poster)*.
- [14] Youngjoon Kwon, Dahun Kim, Duygu Ceylan, and Henry Fuchs. 2021. Neural Human Performer: Learning Generalizable Radiance Fields for Human Performance Rendering. In *Advances in Neural Information Processing Systems*, Vol. 34. Curran Associates, Inc., 24741–24752.
- [15] John P. Lewis, Matt Corder, and Nickson Fong. 2000. Pose Space Deformation: A Unified Approach to Shape Interpolation and Skeleton-Driven Deformation. In *Proceedings of the 27th Annual Conference on Computer Graphics and Interactive Techniques*. 165–172.
- [16] Zhengqi Li, Simon Niklaus, Noah Snavely, and Oliver Wang. 2021. Neural Scene Flow Fields for Space-Time View Synthesis of Dynamic Scenes. In *CVPR*. 6498–6508.
- [17] Lingjie Liu, Marc Habermann, Viktor Rudnev, Kripasindhu Sarkar, Jiatao Gu, and Christian Theobalt. 2021. Neural Actor: Neural Free-View Synthesis of Human Actors with Pose Control. *ACM Transactions on Graphics (TOG)* 40, 6 (2021), 1–16.
- [18] Stephen Lombardi, Tomas Simon, Jason Saragih, Gabriel Schwartz, Andreas Lehrmann, and Yaser Sheikh. 2019. Neural Volumes: Learning Dynamic Renderable Volumes from Images. *ACM Transactions on Graphics (TOG)* 38, 4 (Aug. 2019), 1–14. arXiv:1906.07751 [cs]
- [19] Matthew Loper, Naureen Mahmood, Javier Romero, Gerard Pons-Moll, and Michael J. Black. 2015. SMPL: A Skinned Multi-Person Linear Model. *ACM Transactions on Graphics (TOG)* 34, 6 (2015), 1–16.
- [20] Nelson Max. 1995. Optical Models for Direct Volume Rendering. *IEEE Transactions on Visualization and Computer Graphics* 1, 2 (1995), 99–108.
- [21] Lars Mescheder, Michael Oechsle, Michael Niemeyer, Sebastian Nowozin, and Andreas Geiger. 2019. Occupancy Networks: Learning 3d Reconstruction in Function Space. In *CVPR*. 4460–4470.
- [22] Marko Mihajlovic, Aayush Bansal, Michael Zollhoefer, Siyu Tang, and Shunsuke Saito. 2022. KeypointNeRF: Generalizing Image-based Volumetric Avatars using Relative Spatial Encoding of Keypoints. In *ECCV*.
- [23] Ben Mildenhall, Pratul P. Srinivasan, Matthew Tancik, Jonathan T. Barron, Ravi Ramamoorthi, and Ren Ng. 2021. Nerf: Representing Scenes as Neural Radiance Fields for View Synthesis. *Commun. ACM* 65, 1 (2021), 99–106.
- [24] Thomas Müller, Alex Evans, Christoph Schied, and Alexander Keller. 2022. Instant Neural Graphics Primitives with a Multiresolution Hash Encoding. *ACM Transactions on Graphics (TOG)* 41, 4 (July 2022), 102:1–102:15.
- [25] Atsuhiko Noguchi, Xiao Sun, Stephen Lin, and Tatsuya Harada. 2021. Neural Articulated Radiance Field. In *ICCV*. 5762–5772.
- [26] Jeong Joon Park, Peter Florence, Julian Straub, Richard Newcombe, and Steven Lovegrove. 2019. DeepSDF: Learning Continuous Signed Distance Functions for Shape Representation. In *CVPR*. 165–174.
- [27] Keunhong Park, Utkarsh Sinha, Jonathan T. Barron, Sofien Bouaziz, Dan B. Goldman, Steven M. Seitz, and Ricardo Martin-Brualla. 2021. Nerfies: Deformable Neural Radiance Fields. In *ICCV*. 5865–5874.
- [28] Adam Paszke, Sam Gross, Soumith Chintala, Gregory Chanan, Edward Yang, Zachary DeVito, Zeming Lin, Alban Desmaison, Luca Antiga, and Adam Lerer. 2017. Automatic differentiation in PyTorch. (2017).
- [29] Sida Peng, Junting Dong, Qianqian Wang, Shangzhan Zhang, Qing Shuai, Xiaowei Zhou, and Hujun Bao. 2021. Animatable Neural Radiance Fields for Modeling Dynamic Human Bodies. In *ICCV*. 14314–14323.
- [30] Sida Peng, Yuanqing Zhang, Yinghao Xu, Qianqian Wang, Qing Shuai, Hujun Bao, and Xiaowei Zhou. 2021. Neural Body: Implicit Neural Representations with Structured Latent Codes for Novel View Synthesis of Dynamic Humans. In *CVPR*. 9054–9063.
- [31] Albert Pumarola, Enric Corona, Gerard Pons-Moll, and Francesc Moreno-Noguer. 2021. D-Nerf: Neural Radiance Fields for Dynamic Scenes. In *CVPR*. 10318–10327.
- [32] Amit Raj, Julian Tanke, James Hays, Minh Vo, Carsten Stoll, and Christoph Lassner. 2021. Anr: Articulated Neural Rendering for Virtual Avatars. In *CVPR*. 3722–3731.
- [33] Amit Raj, Michael Zollhoefer, Tomas Simon, Jason Saragih, Shunsuke Saito, James Hays, and Stephen Lombardi. 2021. Pva: Pixel-aligned Volumetric Avatars. *arXiv preprint arXiv:2101.02697* (2021). arXiv:2101.02697
- [34] Shunsuke Saito, Zeng Huang, Ryota Natsume, Shigeo Morishima, Angjoo Kanazawa, and Hao Li. 2019. Pifu: Pixel-aligned Implicit Function for High-Resolution Clothed Human Digitization. In *ICCV*. 2304–2314.
- [35] Shunsuke Saito, Tomas Simon, Jason Saragih, and Hanbyul Joo. 2020. Pifuhd: Multi-level Pixel-Aligned Implicit Function for High-Resolution 3d Human Digitization. In *CVPR*. 84–93.
- [36] Karen Simonyan and Andrew Zisserman. 2015. Very Deep Convolutional Networks for Large-Scale Image Recognition. In *ICLR*.
- [37] Vincent Sitzmann, Michael Zollhöfer, and Gordon Wetzstein. 2019. Scene Representation Networks: Continuous 3d-Structure-Aware Neural Scene Representations. *Advances in Neural Information Processing Systems* 32 (2019).
- [38] Shih-Yang Su, Frank Yu, Michael Zollhöfer, and Helge Rhodin. 2021. A-Nerf: Articulated Neural Radiance Fields for Learning Human Shape, Appearance, and Pose. *Advances in Neural Information Processing Systems* 34 (2021), 12278–12291.
- [39] Matthew Tancik, Pratul Srinivasan, Ben Mildenhall, Sara Fridovich-Keil, Nithin Raghavan, Utkarsh Singhal, Ravi Ramamoorthi, Jonathan Barron, and Ren Ng. 2020. Fourier Features Let Networks Learn High Frequency Functions in Low Dimensional Domains. *Advances in Neural Information Processing Systems* 33 (2020), 7537–7547.
- [40] Edgar Tretschk, Ayush Tewari, Vladislav Golyanik, Michael Zollhöfer, Christoph Lassner, and Christian Theobalt. 2021. Non-Rigid Neural Radiance Fields: Reconstruction and Novel View Synthesis of a Dynamic Scene from Monocular Video. In *ICCV*. 12959–12970.
- [41] Alex Trevithick and Bo Yang. 2021. Grf: Learning a General Radiance Field for 3d Representation and Rendering. In *ICCV*. 15182–15192.
- [42] Qianqian Wang, Zhicheng Wang, Kyle Genova, Pratul P. Srinivasan, Howard Zhou, Jonathan T. Barron, Ricardo Martin-Brualla, Noah Snavely, and Thomas Funkhouser. 2021. IBRnet: Learning Multi-View Image-Based Rendering. In *CVPR*. 4690–4699.
- [43] Yiming Wang, Qingzhe Gao, Libin Liu, Lingjie Liu, Christian Theobalt, and Baoquan Chen. 2022. Neural Novel Actor: Learning a Generalized Animatable Neural Representation for Human Actors. arXiv:2208.11905 [cs]
- [44] Chung-Yi Weng, Brian Curless, Pratul P. Srinivasan, Jonathan T. Barron, and Ira Kemelmacher-Shlizerman. 2022. Humannerf: Free-viewpoint Rendering of Moving People from Monocular Video. In *CVPR*. 16210–16220.
- [45] Minye Wu, Yuehao Wang, Qiang Hu, and Jingyi Yu. 2020. Multi-View Neural Human Rendering. In *CVPR*. 1682–1691.
- [46] Ze Yang, Shenlong Wang, Sivabalan Manivasagam, Zeng Huang, Wei-Chiu Ma, Xinchun Yan, Ersin Yumer, and Raquel Urtasun. 2021. S3: Neural Shape, Skeleton, and Skinning Fields for 3d Human Modeling. In *CVPR*. 13284–13293.
- [47] Lior Yariv, Jiatao Gu, Yoni Kasten, and Yaron Lipman. 2021. Volume Rendering of Neural Implicit Surfaces. *Advances in Neural Information Processing Systems* 34 (2021), 4805–4815.

- [48] Alex Yu, Vickie Ye, Matthew Tancik, and Angjoo Kanazawa. 2021. Pixelnerf: Neural Radiance Fields from One or Few Images. In *CVPR*. 4578–4587.
- [49] Jing Zhang and Dacheng Tao. 2020. Empowering things with intelligence: a survey of the progress, challenges, and opportunities in artificial intelligence of things. *IEEE Internet of Things Journal* 8, 10 (2020), 7789–7817.
- [50] Fuqiang Zhao, Wei Yang, Jiakai Zhang, Pei Lin, Yingliang Zhang, Jingyi Yu, and Lan Xu. 2022. HumanNeRF: Efficiently Generated Human Radiance Field from Sparse Inputs. In *CVPR*. 7743–7753.
- [51] Y. Zhi, S. Qian, X. Yan, and S. Gao. 2022. Dual-Space NeRF: Learning Animatable Avatars and Scene Lighting in Separate Spaces. In *2022 International Conference on 3D Vision (3DV)*. IEEE Computer Society, Los Alamitos, CA, USA, 1–10.